International Journal of Environmental Science and Technology (2023) 20:2021–2036
https://doi.org/10.1007/s13762-022-04101-2

ORIGINAL PAPER

NiO and Ag–Cd co-doped NiO nanoparticles: study of photocatalytic degradation of rhodamine B dye for wastewater treatment

M. Shakil[1] · Usama Inayat[1] · M. Tanveer[1] · G. Nabi[1] · S. S. A. Gillani[2] · M. Rafique[3] · N. H. Tariq[4] · A. Shah[5] · A. Mahmood[5]

Received: 23 March 2021 / Revised: 17 January 2022 / Accepted: 13 March 2022 / Published online: 11 April 2022

Abstract

For the first time, NiO and Ag–Cd co-doped NiO $Cd_xAg_{0.30}Ni_{0.70-x}O$ ($X = 0.0$, 0.05, 0.10, and 0.15) have been synthesized through a facile sol–gel method to investigate the photocatalytic performance by visible-light-driven degradation of rhodamine B dye for wastewater treatment. All samples were characterized through X-ray diffraction, field emission scanning electron microscopy, energy-dispersive X-ray, Fourier transform infrared, photoluminescence, and ultraviolet–visible spectroscopy for structural, morphological, elemental, functional groups, optical, and bandgap analysis, respectively. Face-centered cubic structure of NiO was confirmed through X-ray diffraction. The formation of NiO and Ag–Cd co-doped NiO nanoparticles was confirmed through elemental and functional groups analysis. Optical properties obtained from photoluminescence spectroscopy revealed visible-light emission spectrum and slower electron/hole pair recombination rate with an increase in doping. Minimum optical bandgap energy of 2.37 eV was found for the $Cd_{0.15}Ag_{0.30}Ni_{0.55}O$ sample. Photocatalytic performance study revealed that degradation followed first-order kinetics. $Cd_{0.15}Ag_{0.30}Ni_{0.55}O$ was the best sample which showed the maximum efficiency of 97%, the reaction rate constant K (min^{-1}) of 0.0496, and the correlation coefficient (R^2) of 0.988 after 140-min degradation of rhodamine B dye. The reusability and stability of the best sample were checked for six cycles by obtaining an X-ray diffraction pattern after the photocatalytic process.

Keywords Bandgap energy · Electron/hole pair recombination · Photocatalysis · Photoluminescence · Reaction rate constant · Reusability

Introduction

In recent years with the invention of technology and enhancement in different aspects of science, man has gained many benefits. Humans all across the globe are facing the water pollution, one of the major problems of humanity. With the increase in industrial areas, water pollution has become a dangerous element for humans, animals, and organisms living in water (Ahmed et al. 2017). One study reported previously has revealed that annually 0.7 million tons of synthetic dyes is being produced and 15% of the total production of these dyes is being discharged and poured into the water by different industries including paint, food, cosmetics, paper, and textile (Anwer et al. 2019). Discharge of dyes into water is extremely hazardous to the aquatic organisms and for humans. Another study has revealed that more than 4 million children are affected daily due to wastewater-caused diseases. Furthermore, it has also been reported that more than 1.2 billion people across the world have no access to pure water (Mansour

Editorial responsibility: Senthil Kumar Ponnusamy.

✉ M. Shakil
shakil101@yahoo.com

[1] Department of Physics, University of Gujrat, Gujrat 50700, Pakistan

[2] Department of Physics, Government College University Lahore, Lahore 54000, Pakistan

[3] Department of Physics, University of Sahiwal, Sahiwal, Pakistan

[4] Department of Metallurgy and Materials Engineering, Institute of Engineering and Applied Sciences (PIEAS), P.O, Nilore, Islamabad, Pakistan

[5] National Institute of Lasers and Optronics (NILOP), P.O Nilore, Islamabad, Pakistan

et al. 2020). Not only dyes are contaminating water, but there are other toxic pollutants including pesticides, heavy metals, compounds containing phenol, microplastics, and pharmaceutical compounds (Rosenwinkel et al. 2005; Ma et al. 2009; Owa 2013; Palma et al. 2010; Puckett 1995).

The reported data on water pollutants indicated that the development of an efficient, eco-friendly, reliable, and cost-effective method is needed to purify polluted water. Different methods were adopted by researchers to clean the water in past (Choudri et al. 2020; Shannon et al. 2010; Yongabi 2010). These methods include advanced oxidation process, flocculation, ion exchange, biological treatment, coagulation, sedimentation, adsorption, and membrane filtration (Crini and Lichtfouse 2019; Gogate and Pandit 2004; van Loosdrecht et al. 2016). Among these methods, the advanced oxidation process is the most effective process to degrade water contaminations by of reduction and oxidation (Ghernaout 2020; Khan et al. 2020). Among advanced oxidation processes, the photocatalysis is considered as the reliable process. The photocatalysis process works on the principle of the production of radicals that react with the pollutants in water and oxidize them (Sacco et al. 2018).

With the enhancement in research, different materials have gained attention due to their potential application as photocatalysts. Synthesized semiconductor photocatalysts are being investigated by researchers for dyes removal from wastewater (Ge et al. 2019). *N*-type and *p*-type semiconductors are being investigated for photocatalysis application which includes NiO, Fe_2O_3 and ZnO, TiO_2, respectively (Medhi et al. 2020). *N*-type semiconductor TiO_2 was the first material used as photocatalyst for wastewater treatment (Hussain et al. 2010).

Among different transition metal oxide *p*-type semiconductors, NiO is one of the active materials for different applications such as gas sensors, photocatalyst, magnetic storage devices, and solar cells due to prominent electrical properties, magnetic properties, optical properties, eco-friendly, less toxic, high chemical and thermal stability, economical, easy to synthesize, and photosensitive nature. NiO has wide gap ranges from 3.2 to 4 eV having cubic crystal structure FCC with lattice constant "a" 4.17 Å and space group Fm3m (Arif et al. 2019; Sheena et al. 2014). Due to the wide bandgap of NiO, these materials are less efficient for dyes degradation in visible light because wide bandgap possesses high electron/hole pair recombination rate. Doping is a method that changes the structure, shape, and optical properties of host materials due to different properties of dopant material as compared to host material (Shakil et al. 2020). To bring the NiO in the visible range for photocatalysis and make it efficient material for photocatalysis, its bandgap is required to decrease by doping as one of the methods with different dopants (Hussain et al. 2021). By doping transition metals in NiO such as Cd, Ag, Co, Bi, and Fe, the bandgap of the NiO can be tuned remarkably (Al-Sehemi et al. 2014; Sagadevan and Podder 2015). By altering structural and optical properties of NiO through the doping process, higher efficiency of photocatalysis as compared to NiO is achieved (Khairnar and Shrivastava 2019).

Investigation of NiO and doped NiO as photocatalyst is one of the active topics in research currently. Ranjbar et al. have synthesized NiO nanoparticles through solid-state thermal reaction by decomposing nanostructures of nickel acetate which was obtained through powder nickel acetate sublimation. Effect of temperature of sublimation was investigated for NiO nanoparticles at four different temperatures. Cubic particles having average crystallite size in the range of 30 to 50 nm were observed through XRD analysis. Degradation of MB dye was investigated under visible-light irradiation. It was observed that NiO sample prepared at 350 °C temperature has greater efficiency of degradation up to 98% while decolorizing MB dye after 120-min irradiation (Ranjbar et al. 2015). Diallo et al. investigated the biosynthesized NiO particles for decolorization of MB dye under UV light and visible light. Average crystallite size 14 nm was calculated and confirmed for cubic NiO prepared samples through XRD, HRTEM, and FTIR studies. It was observed that biosynthesized NiO nanoparticles were effectively capable of degrading MB dye under suitable light irradiation (Diallo et al. 2018). Muhammad Imran et al. have adopted a green synthesis approach to synthesize Ni and NiO nanoparticles for photocatalysis application by using Hordeum vulgare seeds as a capping agent. It has been observed that the green synthesis prepared NiO is an efficient photocatalyst to degrade MB dye which followed first-order kinetics (Din et al. 2020). Ghazal et al. synthesized silver-doped NiO nanoparticles through Cydonia oblonga plant extract-mediated sol–gel technique. Several properties were observed and revealed through appropriate techniques for the confirmation of the prepared samples and the application. An increase in particle size of Ag-doped NiO has been observed with the increase in silver concentration revealed by XRD. The photocatalytic application was done by degrading RhB dye under UV light for 3 h and 20 min of irradiation. The result revealed 75% efficiency to remove RhB dye from wastewater for Ag-doped NiO nanoparticles (Ghazal et al. 2020).

In this article, NiO and novel Cd–Ag co-doped NiO, $Cd_xAg_{0.30}Ni_{0.70-x}O$ ($X = 0.0$, 0.05, 0.10 and 0.15) nanoparticles have been synthesized through the sol–gel technique for wastewater treatment through degradation of RhB dye. Structural, morphological, and optical properties were investigated through X-ray diffraction (XRD), field emission scanning electron microscopy (FESEM), energy-dispersive X-ray (EDX), Fourier transform infrared (FTIR), photoluminescence (PL), and ultraviolet–visible (UV–Vis) spectroscopy, respectively. These properties would be highly advantageous for the usage of NiO and co-doped NiO as a photocatalyst in photocatalysis applications.

This work had been carried out at Department of Physics, University of Gujrat, Gujrat, Pakistan, during January–March 2021.

Materials and methods

Materials

For the sol–gel method to synthesize NiO and Ag–Cd co-doped NiO nanoparticles, nickel nitrate hexahydrate ($Ni(NO_3)_2{\cdot}6\ H_2O$), silver nitrate ($AgNO_3$), and cadmium nitrate tetrahydrate ($Cd(NO_3)_2{\cdot}4\ H_2O$) salt precursors were used, while citric acid ($C_6H_8O_7$) was used as the chelating agent. And ammonia (NH_3) solute was utilized to maintain the pH of the samples (Ba-Abbad et al. 2015). All these materials were purchased from Sigma–Aldrich and used without any further purification.

Synthesis of nanoparticles

Synthesis of NiO and Ag–Cd co-doped NiO, $Cd_xAg_{0.30}Ni_{0.70-x}O$ ($X = 0.0$, 0.05, 0.10 and 0.15) has been done by adopting sol–gel method. This technique is eco-friendly, non-toxic, cost-effective, and easy, which gives refined morphologies of the prepared samples. The detail for the preparation of proposed samples is given in the following.

To synthesize NiO, the calculated amount of nickel nitrate was dissolved in distilled water; after that, the calculated amount of citric acid with appropriate ratio with nickel nitrate was dissolved in the prepared salt solution. The mixture was kept at a magnetic stirrer for half an hour, and then, the pH was maintained up to 9–10 by adding ammonia solution dropwise. 180 °C temperature was set after maintaining pH, and the solution was kept at stirring until thick gel was formed. This formed gel was then dried in the open air and ground into fine powder. At last, this fine powder was calcinated at 550 °Ctemperature in a muffle furnace for 4 h and NiO nanoparticles were obtained (Gawali et al. 2016). A similar approach was adopted for the synthesis of Ag-doped NiO, Cd-doped NiO, and Ag–Cd co-doped NiO nanoparticles. The calculated amount of silver nitrate, cadmium nitrate, and nickel nitrate salts will be mixed in distilled water, and the rest will be the same procedure. The flowchart of the whole process is shown in Fig. 1. A similar mechanism was performed for the synthesis of NiO except for the addition of dopant precursors.

Photocatalytic activity

The photocatalytic performance of NiO and Ag–Cd co-doped NiO samples was investigated through the degradation of RhB dye. For degradation purposes, dye solution was made by adding 2 ppm RhB dye in 50 mL distilled water. After that, 10 mg of each sample was added to the 50 mL dye solution separately in five beakers. To attain adsorption/desorption equilibrium, the solution was stirred in dark for half an hour. After half an hour, 5 mL solution was taken, and absorption spectra were obtained which is zero-time absorbance. After that, the solution was exposed to visible light (homemade metal halide photocatalysis reactor of 400 W power) and degradation was checked by collecting 5 mL solution after 20 min through a UV-1800 ultraviolet–visible spectroscope. The whole process of photocatalysis was performed for 2 h and 20 min. The RhB concentration was examined through absorption spectra of all degraded samples at 552 nm wavelength, and the calibration curve was plotted as shown in Fig. 2. The correlation coefficient (R^2) was determined also.

The percentage degradation efficiency was calculated using the following formula (Tahir et al. 2020b):

$$\%\ \text{degradation} = \left[1 - C/C_0\right] \times 100. \tag{1}$$

Here, C_0 is the concentration of solution without light irradiation and C is the concentration at a maximum irradiation time of 140 min.

Rate of reaction for the degradation of RhB was calculated by using the following formula (Malik et al. 2018; Tahir et al. 2018):

$$\ln\left(C_0/C\right) = k \cdot t \tag{2}$$

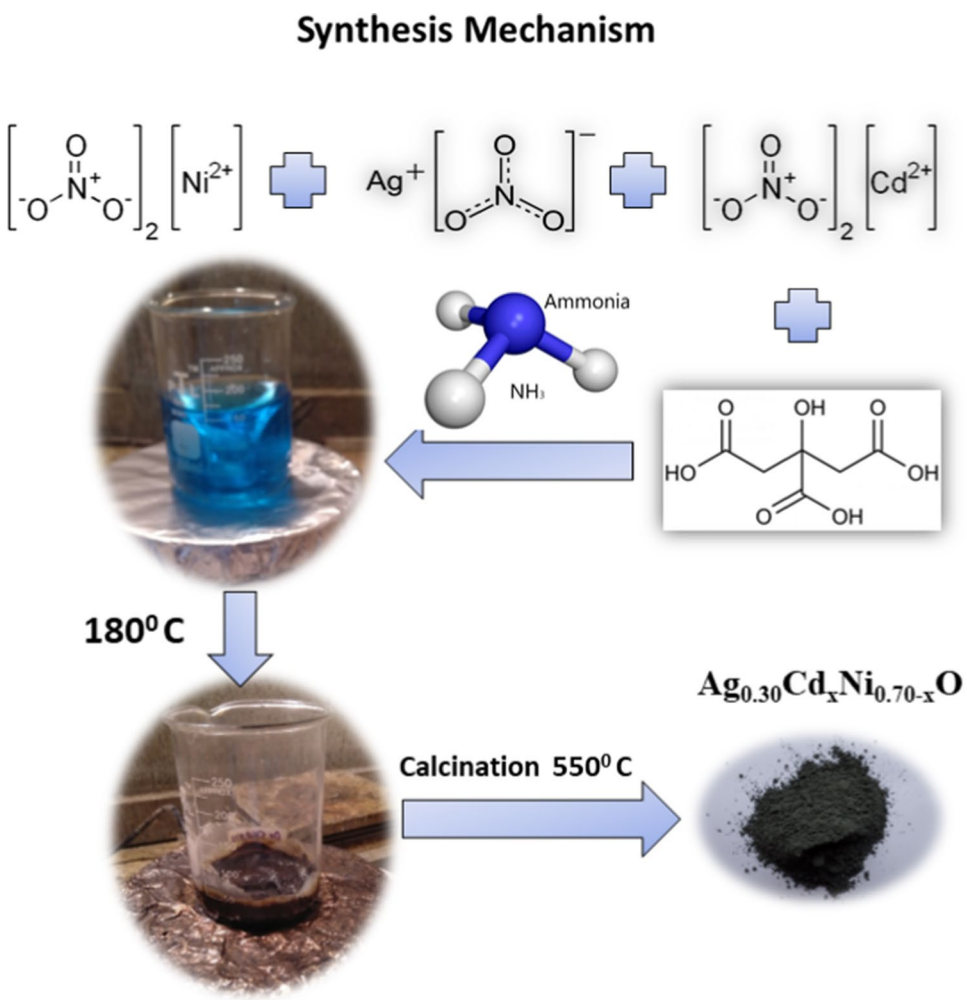

Fig. 1 Flowchart of preparation of Ag–Cd co-doped NiO nanoparticles

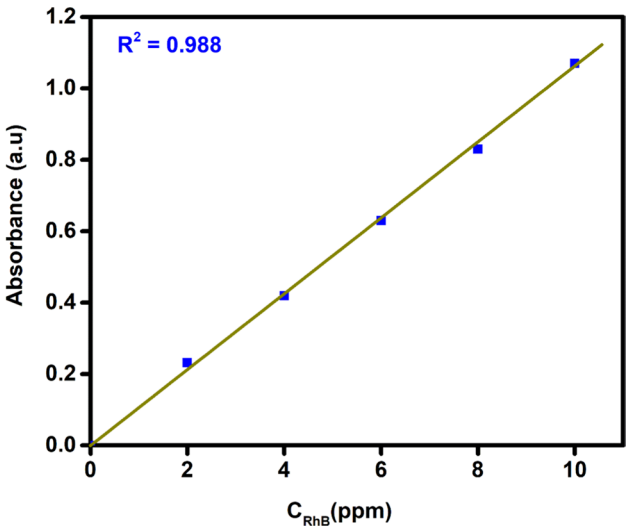

Fig. 2 Calibration curve of RhB dye

where k is called the reaction rate constant and t is the irradiation time.

Characterization techniques

X-ray diffraction technique (Bruker D8) with Cu-kα ($\lambda = 1.541874$ Å) with a step of 20/min was used for investigation of structural properties in 2θ range 30°–90°. Characterization of elemental analysis and surface morphology of the synthesized samples was done utilizing field emission scanning electron microscopy (TESCAN MAIA3). Fourier transform infrared (FTIR-4100 type-A, JASCO) spectroscopy was employed to reveal the presence of functional groups in samples. Emission spectra were obtained through photoluminescence spectroscopy (FP-8200 spectrofluorometer, JASCO) in the range of 380 nm to 500 nm with 380 nm excitation wavelength. Finally, bandgap energy and photocatalytic activity were investigated through a UV-1800 ultraviolet–visible spectroscope.

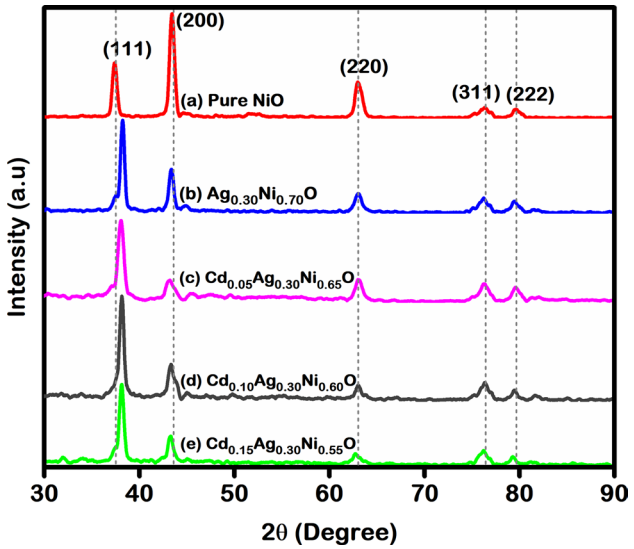

Fig. 3 XRD graph of NiO and Ag–Cd co-doped NiO, $Cd_xAg_{0.30}Ni_{0.70-x}O$ ($X = 0.0$, 0.05, 0.10, and 0.15) nanoparticles

Results and discussion

Structural analysis

X-ray diffraction technique was utilized to investigate the structural properties of the prepared samples. XRD graph of NiO and Ag–Cd co-doped NiO is shown in Fig. 3. In this graph, five peaks in the range of 30°–90° can be observed which were indexed as (111), (200), (220), (311), and (222),

Table 1 Average crystallite sizes of the prepared samples of NiO and Ag–Cd co-doped NiO nanoparticles

Samples	Average crystallite size "d" (nm)	Lattice parameter "a" (Å)
NiO	28	4.1772
$Ag_{0.30}Ni_{0.70}O$	29	4.1753
$Cd_{0.05}Ag_{0.30}Ni_{0.65}O$	26	4.1742
$Cd_{0.10}Ag_{0.30}Ni_{0.60}O$	25	4.1701
$Cd_{0.15}Ag_{0.30}Ni_{0.55}O$	24	4.1679

respectively. This XRD peaks are well consistent with Joint Committee on Powder Diffraction Standards (JCPDS) card no. 78–0643 which revealed the formation of the cubic structure of all prepared samples having space group Fm-3 m (Dehno Khalaji 2015). It has been observed that the peaks were slightly shifted toward a higher angle and the intensity of peaks was also decreased with an increase in doping. This behavior is evidence of Ag and Cd co-doping in NiO (Ahmed and Nabi 2020). A decrease in intensity improved the crystallinity of doped samples. The average crystallite size was determined using the Debye–Scherrer formula through full width at half maxima (FWHM) of the observed peaks (Table 1).

The average crystallites size of NiO was 28 nm. It has been observed that the crystallite size was increased with Ag doping from 28 to 29 nm but decreased again with Cd doping. Also, the lattice parameter 'a' was decreased with an increase in doping. This decrement can be ascribed to few aspects, including greater ionic radii of Cd and Ag as compared to Ni, production of interstitial and vacancy defects due to doping and strain due to temperature (Al Boukhari et al. 2020). The average crystallite sizes and lattice parameters are shown in Table 1. Further, no additional peak was observed in all samples which is an indication of the purity of all samples. High crystallinity and smaller crystallite sizes of these materials lead to the prediction that these samples can be utilized as photocatalysts. These XRD results are matched with previously reported studies of NiO and doped NiO nanoparticles (Dehno Khalaji 2015; Kannan et al. 2020; Kerli et al. 2020; Ethiraj et al. 2020).

Morphological analysis

FESEM was employed to investigate surface morphologies of the prepared samples. The FESEM images of NiO and Ag–Cd co-doped NiO are shown in Fig. 4. It is seen that the NiO has cubic-shaped particles, confirming its FCC structure and in good agreement with XRD data, while upon doping the surface morphologies of doped NiO changed from cubic-like particles to spherical-shaped particles which changed due to greater ionic radii of Ag and Cd as compared to Ni. Agglomeration can be observed in all samples as shown in Fig. 4. Agglomeration was increased with doping due to intermolecular forces and the magnetic interaction of particles (Mohammadyani et al. 2012). Also, this agglomeration is evidence of greater surface-to-volume ratios of the prepared samples which is essential for photocatalysis, because as the surface-to-volume ratio increases the surface energy gets high, to minimize this energy nanoparticle gets agglomerated (Deng and Davé 2017; Jiang et al. 2009; Pellegrino et al. 2017).

Elemental analysis

Elemental analysis was performed through the EDX technique which confirmed the presence of Ni, O, Ag, and Cd. EDX spectra are shown in Fig. 5.

FTIR

Functional groups analysis is important to study the verification of the sample preparation. FTIR analysis was performed in the range of 3000 to 500 cm^{-1} to study the presence of functional groups in all prepared samples of NiO and Ag–Cd co-doped NiO, $Cd_xAg_{0.30}Ni_{0.70-x}O$ ($X = 0.0$, 0.2, 0.6 and 1.0). IR spectra for all samples are shown in Fig. 6. It has been observed that there are five broader and weaker peaks in the range of 500 to 1500 cm^{-1} in all compositions. The peaks at 1392 cm^{-1} and 1434 cm^{-1} were because of bending vibrations of the O–H group as samples absorbed water molecules or due to the interaction of samples with KBr (Aslam et al. 2021; Diallo et al. 2018). Similarly, the peaks at 1051 cm^{-1}, 1085 cm^{-1}, and 1115 cm^{-1} are attributed to symmetrical stretching of nitro compound N–O (Zahra et al. 2020).

Likewise, a band at 872 cm^{-1} was due to C–H bending (Arif et al. 2019). The lower frequency band in the range of 850 to 500 was attributed to the stretching vibration of the metal-oxide bond. It can be seen from Fig. 6 that two peaks at 615 cm^{-1} and 533 cm^{-1} wavenumbers were arisen due to Cd–O, Ag–O, and Ni–O bonds, respectively, which confirms M–O bonding presence in all prepared samples. FTIR spectra were well matched with earlier reported data (Fazlali et al. 2015; Ghazal et al. 2020; Torki and Faghihian 2018).

Optical analysis

Optical properties were investigated through PL for all prepared samples of NiO and Ag–Cd co-doped NiO nanoparticles $Cd_xAg_{0.30}Ni_{0.70-x}O$ ($X = 0.0$, 0.05, 0.10, and 0.15) as shown in Fig. 7. PL spectra were obtained for all the samples in a range of 380 to 500 nm with an excitation wavelength of 380 nm. It has been observed that all samples gave emission peaks at 413 nm (3 eV) due to the presence of oxygen vacancies at surfaces (Deshpande et al. 2016). Also, it can be observed that the intensity is decreasing with an increase in doping which is authentication of slow electron/hole pair recombination (Murali et al. 2020). The sample with $X = 0.15$ $Cd_{0.15}Ag_{0.30}Ni_{0.55}O$ shows the lowest intensity peak in which electron/hole pair recombination was much slower than other samples, which indicates that this sample can be used as an efficient photocatalyst.

Bandgap analysis

Bandgap energies of NiO and Ag–Cd co-doped NiO nanoparticles were determined through absorption spectra of UV–Vis spectroscopy, and their respective spectrum is shown in Fig. 8. To obtain bandgap energies, three samples including NiO, $Cd_{0.05}Ag_{0.30}Ni_{0.65}O$, and $Cd_{0.15}Ag_{0.30}Ni_{0.55}O$ were examined under UV–Vis spectroscopy and their energies were calculated through Tauc's plot (Khodair et al. 2020) as shown in Fig. 8a–d, respectively. The Tauc relation is given as follows:

$$(\alpha h\upsilon)^2 = K\,(h\upsilon - E_g)^n. \tag{3}$$

Here, "E_g" is the energy of the bandgap, "$h\upsilon$" is the energy of incident photons, "α" is the coefficient of absorption, "K" is the energy independent constant, and "n" is the transition nature. Since NiO has indirect transition and the value of "n" for indirect transition is 2 (Rahman et al. 2018). The absorption spectrum and $(\alpha h\upsilon)^2$ versus E_g graph of samples are shown in Fig. 8d.

From these spectra, it can be observed that samples show absorption in the visible region and bandgap energies were 3.20 eV, 2.79 eV, and 2.37 eV for samples, NiO, $Cd_{0.05}Ag_{0.30}Ni_{0.65}O$, and $Cd_{0.15}Ag_{0.30}Ni_{0.55}O$, respectively. The decrease in bandgap energies and the increase in Cd co-doping were observed, which might be due to the formation of new additional energy states near to valance band and an increased inhomogeneity and density of localized states (Ahmed and Nabi 2020). Also, bandgap variation can be caused by different crystallite sizes of samples (Khodair et al. 2020). The decrement in the bandgap and the increase in doping are evidences that the Ag–Cd co-doped NiO can be employed as an efficient visible-light-driven photocatalyst. Among all the samples, $Cd_{0.15}Ag_{0.30}Ni_{0.55}O$ has less bandgap energy. The results of these samples are well related to the earlier reported studies (Amor et al. 2017; Hameeda et al. 2020; Khatri and Rana 2020).

Photocatalytic performance

Photocatalysis activity was investigated through the degradation of model organic compound RhB dye. The performance was examined by exposing the solution of RhB and synthesized samples to visible light. Degradation was done followed by decolorization of RhB after exposure to light for 0–140 min with 20 min of interval. UV–Vis spectroscopy was used to study photocatalytic efficiencies of the prepared catalysts by getting absorbance spectra as shown in Fig. 9. Figure 9a shows the absorption spectra of NiO nanoparticles when an aqueous solution of dye was degraded photocatalytically in the presence of light. It has been observed that the absorbance peak was reduced down to 1.275 after 140 min of irradiation and showed 24% efficiency calculated from Eq. (1). Figure 9b shows the absorption spectrum of $Ag_{0.30}Ni_{0.70}O$ particles which showed 39% efficiency after 140 min. The absorption peak was decreased down

Table 2 Photocatalytic performance comparison of doped NiO samples

Samples	Dyes	Irradiation Time (Minutes)	Irradiation Light	Efficiency (%)	References
NiO	MB	180	Visible	59	Kerli et al. (2020)
Ag-doped NiO	RhB	200	UV	75	Ghazal et al. (2020)
Cu-doped NiO	Phenol	150	UV	85.7	Ethiraj et al. (2020)
Cu-doped NiO	AR	30	Visible	> 90	Hameeda et al. (2020)
Co-doped NiO	MB	150	Visible	85	Khatri and Rana (2019)
Ag–Cd co-doped NiO	RhB	140	Visible	97	This study

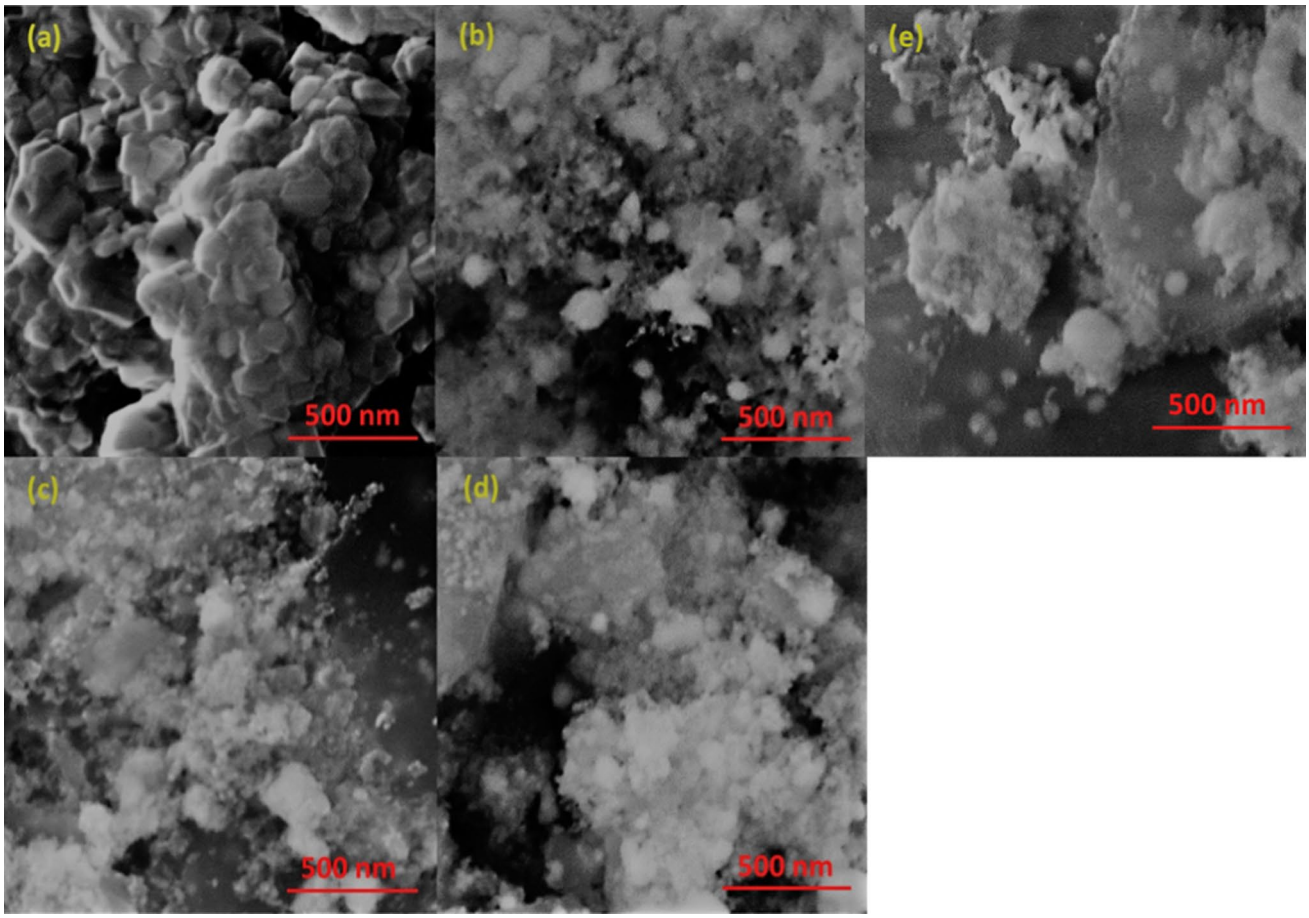

Fig. 4 FESEM images of the prepared samples: **a** NiO, **b** $Ag_{0.30}Ni_{0.70}O$, **c** $Cd_{0.05}Ag_{0.30}Ni_{0.65}O$, **d** $Cd_{0.10}Ag_{0.30}Ni_{0.60}O$, **e** $Cd_{0.15}Ag_{0.30}Ni_{0.55}O$

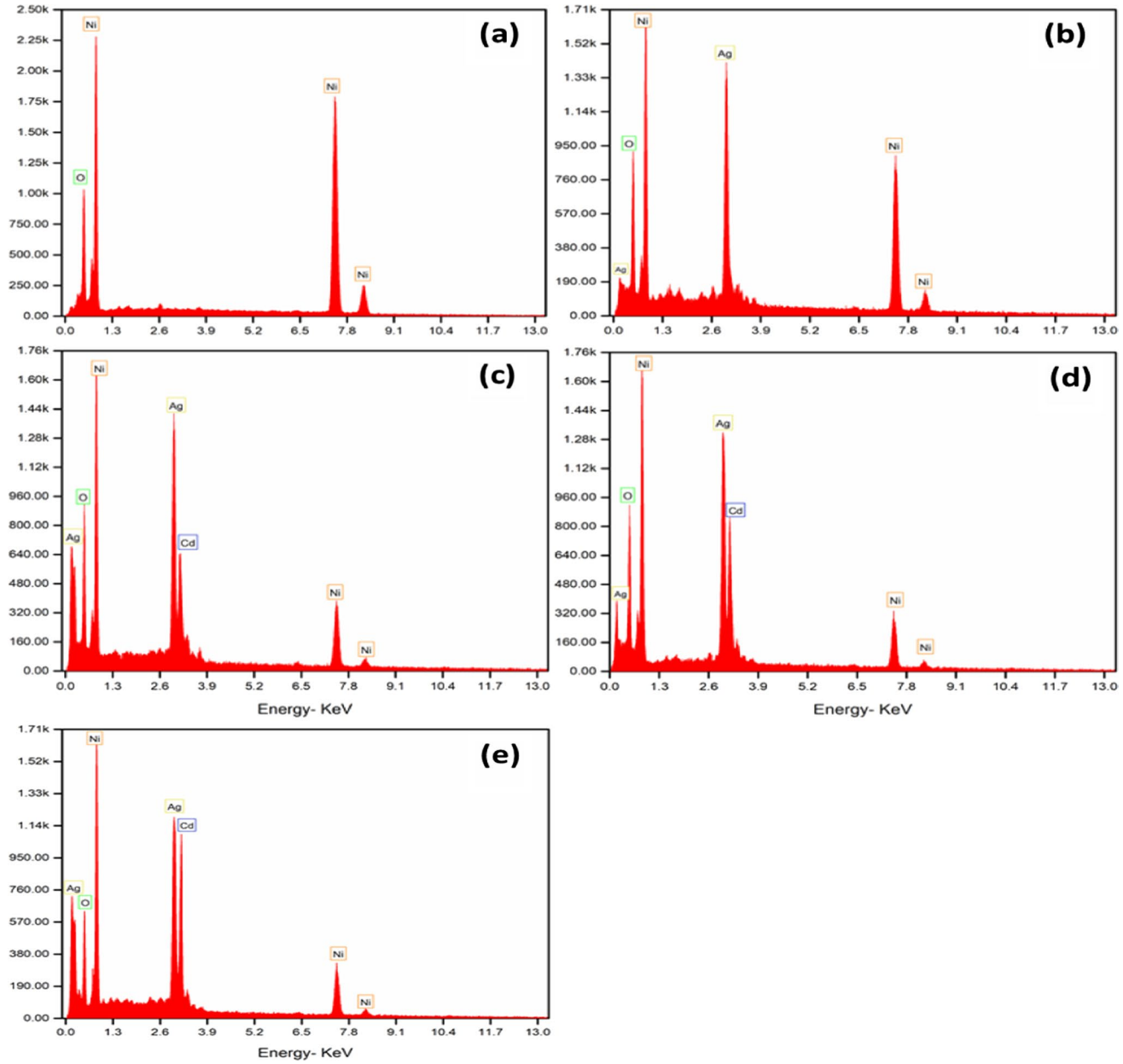

Fig. 5 EDX graphs of **a** NiO, **b** $Ag_{0.30}Ni_{0.70}O$, **c** $Cd_{0.05}Ag_{0.30}Ni_{0.65}O$, **d** $Cd_{0.10}Ag_{0.30}Ni_{0.60}O$, **e** $Cd_{0.15}Ag_{0.30}Ni_{0.55}O$

to 0.975. Similarly, Fig. 9c shows the absorption spectra of $Cd_{0.05}Ag_{0.30}Ni_{0.65}O$ which was 58% efficient for degrading RhB dye, and the absorption peak was decreased down to 0.618. Figure 9d shows the spectrum of $Cd_{0.10}Ag_{0.30}Ni_{0.60}O$ nanoparticles, and it can be observed that the absorption peak was further decreased down to 0.262 and showed 79% efficiency when Cd doping increased. Figure 9e shows the last sample $Cd_{0.15}Ag_{0.30}Ni_{0.55}O$ absorption spectrum whose absorbance was decreased significantly down to 0.003 after 140-min irradiation and showed maximum efficiency of 97%. From these spectra, it can be observed that the efficiencies are being increased while increasing Cd co-doping. $Cd_{0.15}Ag_{0.30}Ni_{0.55}O$ showed the maximum degradation efficiency of 97%.

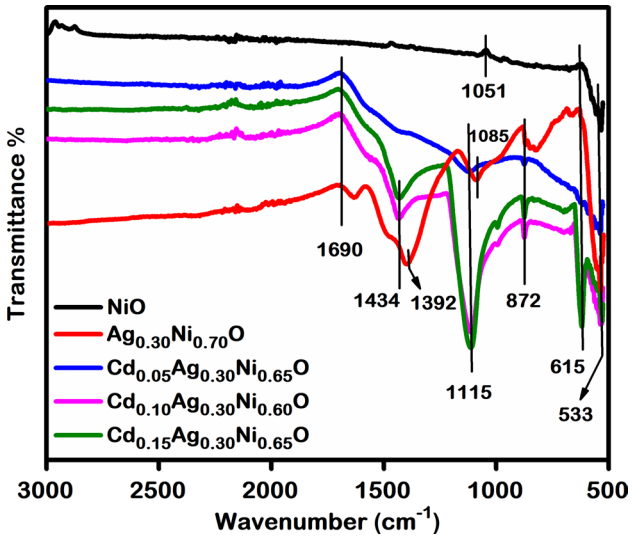

Fig. 6 FTIR graph of NiO and Ag–Cd co-doped NiO, $Cd_xAg_{0.30}Ni_{0.70-x}O$ ($X = 0.0$, 0.05, 0.10, and 0.15) nanoparticles

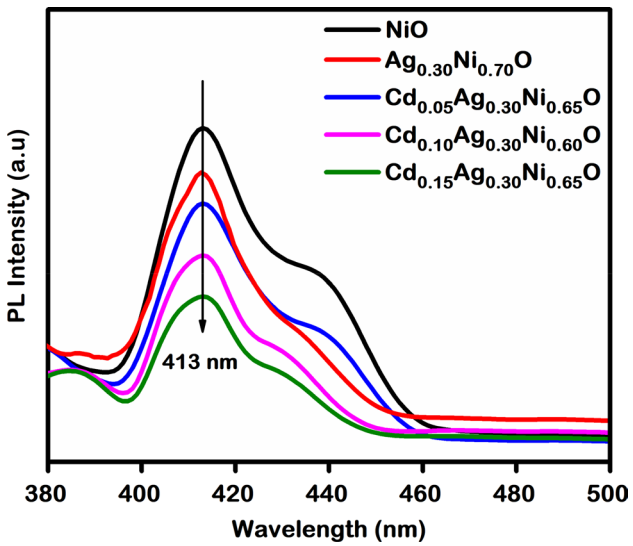

Fig. 7 PL spectra of NiO and Ag–Cd co-doped NiO, $Cd_xAg_{0.30}Ni_{0.70-x}O$ ($X = 0.0$, 0.05, 0.10, and 0.15) nanoparticles

The possible reasons for greater efficiency might be that this sample has smaller crystallite size as can be seen from XRD, slower electron/hole pair recombination as compared to other samples, and reduced bandgap energy 2.37 eV as can be shown in PL and UV–Vis spectra, respectively (Bashir et al. 2021; Anandan and Rajendran 2015). Efficiencies of all samples are shown graphically in Fig. 9f.

Many researchers have been working on photocatalysis application of NiO and doped NiO as an effective photocatalyst, but this proposed work of NiO and Ag–Cd co-doped NiO, $Cd_xAg_{0.30}Ni_{0.70-x}O$ ($X = 0.0$, 0.05, 0.10, and 0.15) is more efficient. Table 2 is incorporated which includes the comparison study of photocatalytic performances between other doped NiO materials and this work. Ethiraj, A.S., et al. (Ethiraj et al. 2020) studied the 2–4 wt.% Cu-doped NiO particles for phenolic compounds degradation. It was found that 2% Cu-doped NiO showed 85.7% efficiency, while degradation was due to a low concentration of phenol. Hameeda et al. (2020) have investigated the degradation of alizarin red (AR) using Cu-doped NiO nanocatalyst. 20% Cu-doped NiO showed the maximum degradation efficiency due to higher surface area 165.6 m^2/g and lower bandgap energy 3.21 eV. Similarly, Khatri and Rana (2019) investigated the degradation of methylene blue (MB) dye using Co-doped NiO photocatalysts. It was observed that $Ni_{0.6}Co_{0.4}O$ degraded MB dye in 50 min with the highest degradation efficiency, which could be due to the reason of enhancement of Co doping which affects the bandgap of NiO. With comparison to these results, it is clear that Ag–Cd co-doped NiO has higher degradation efficiency as compared to other doped NiO nanoparticles.

The kinetic properties were studied by plotting ln (C_0/C) versus irradiation time as shown in Fig. 10a. It can be seen that linear plots are obtained by plotting absorbance data as ln (C_0/C) versus irradiation time. From this graph, it can be concluded that these samples exhibit pseudo-first-order rate reaction, and rate reaction constant K per min is calculated accordingly as shown in Fig. 10b. The value of K (min^{-1}) for NiO was 0.01131. The rate reaction constant was increased with an increase in co-doping of Cd, and maximum reaction rate constant K (min^{-1}) 0.0496 was determined for the $Cd_{0.15}Ag_{0.30}Ni_{0.55}O$ sample, which is 4.39 times greater than the rate reaction constant value of NiO. The correlation coefficient R^2 for the $Cd_{0.15}Ag_{0.30}Ni_{0.55}O$ sample was calculated at 0.988. Moreover, the reusability of the most efficient sample $Cd_{0.15}Ag_{0.30}Ni_{0.55}O$ was checked for six cycles as shown in Fig. 10c. Particles were separated through the centrifugation process. The nanoparticles can also be separated through dye solution through magnets at a large scale as reported in previous studies (Chen et al. 2019; Shekofteh-Gohari and Habibi-Yangjeh 2017; Palanivel et al. 2021; Rahman et al. 2020; Gebreslassie et al. 2019). The efficiency was found 95% after the sixth cycle, and no significant loss was determined. At last, an XRD pattern was obtained for the used sample after the sixth cycle as shown in Fig. 10d. It can be noticed that peaks intensity was reduced slightly after photocatalysis. These results may be due to the adsorption of dye on the surface of the catalyst (Bibi et al. 2018). These results confirmed the reusability and sustainability of our best sample.

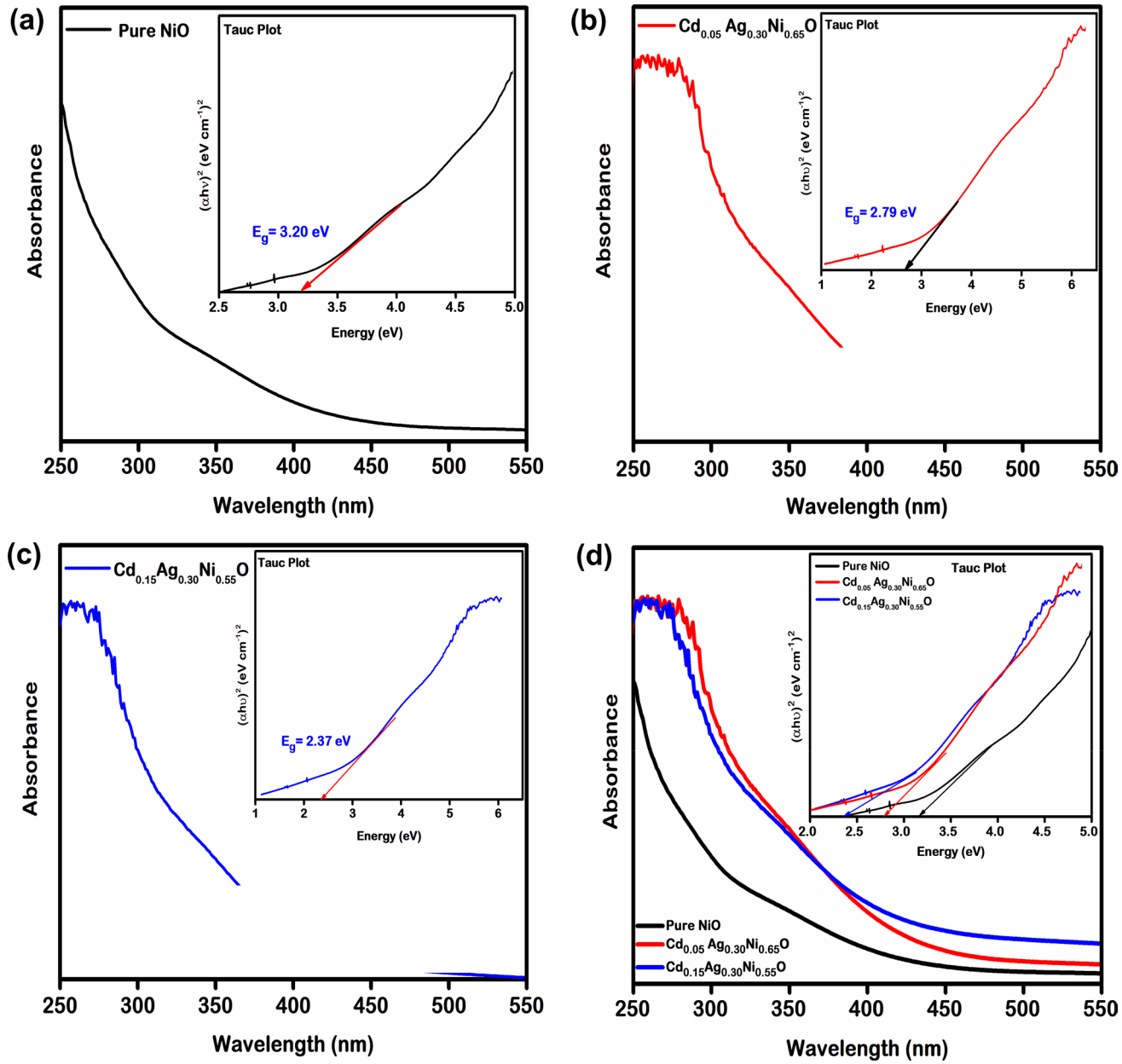

Fig. 8 Absorption spectra and Tauc's plot of samples: **a** NiO, **b** $Cd_{0.05}Ag_{0.30}Ni_{0.65}O$, **c** $Cd_{0.15}Ag_{0.30}Ni_{0.55}O$, **d** absorption spectra and Tauc's plot of all samples

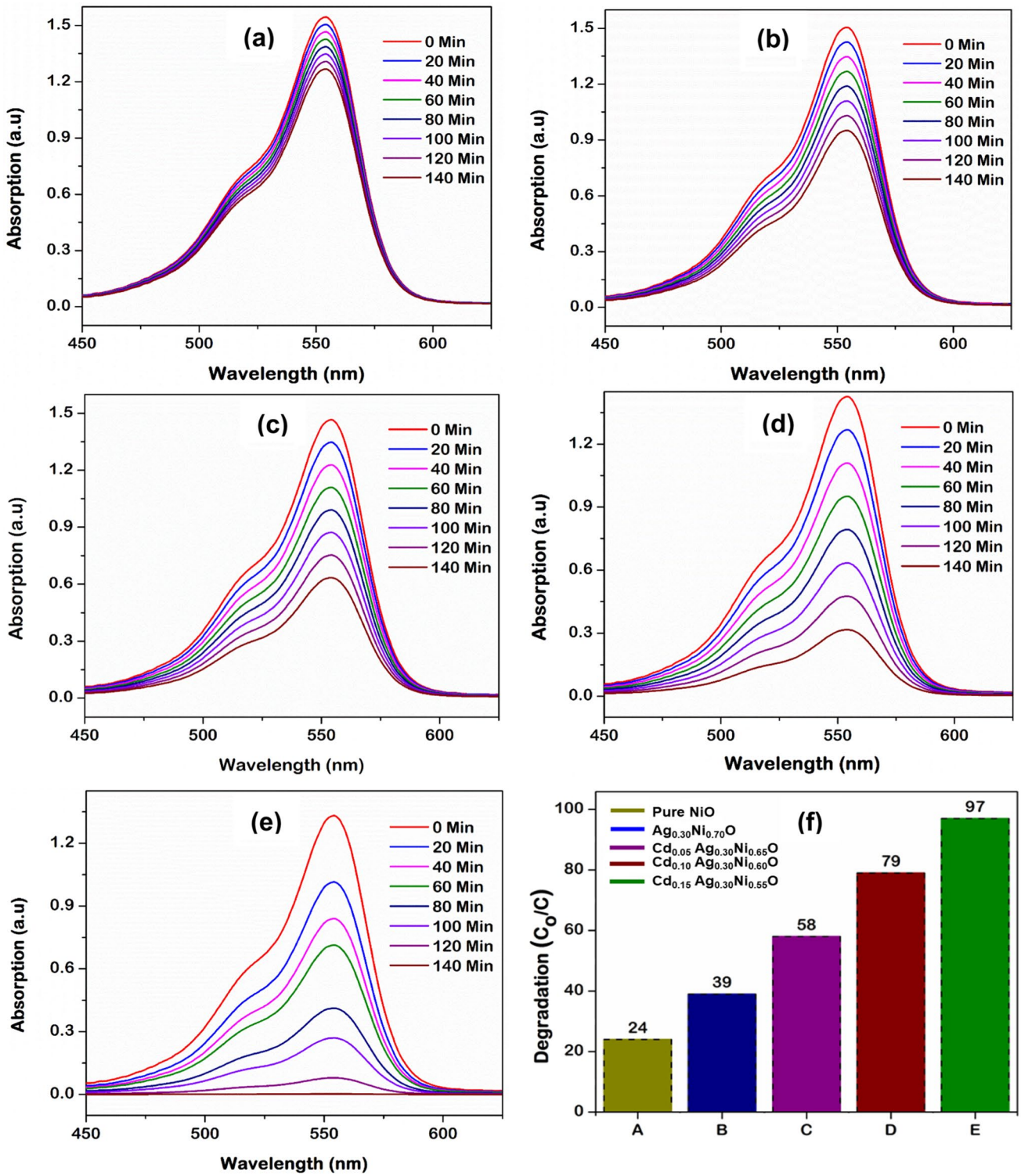

Fig. 9 Photocatalysis UV-Vis spectra of prepared samples **a** pure NiO **b** ag0.30Ni0.70O, **c** $Cd_{0.05}Ag_{0.30}Ni_{0.65}O$ **d** $Cd_{0.10}Ag_{0.30}Ni_{0.60}O$ **e** $Cd_{0.15}Ag_{0.30}Ni_{0.55}O$ **f** efficiencies

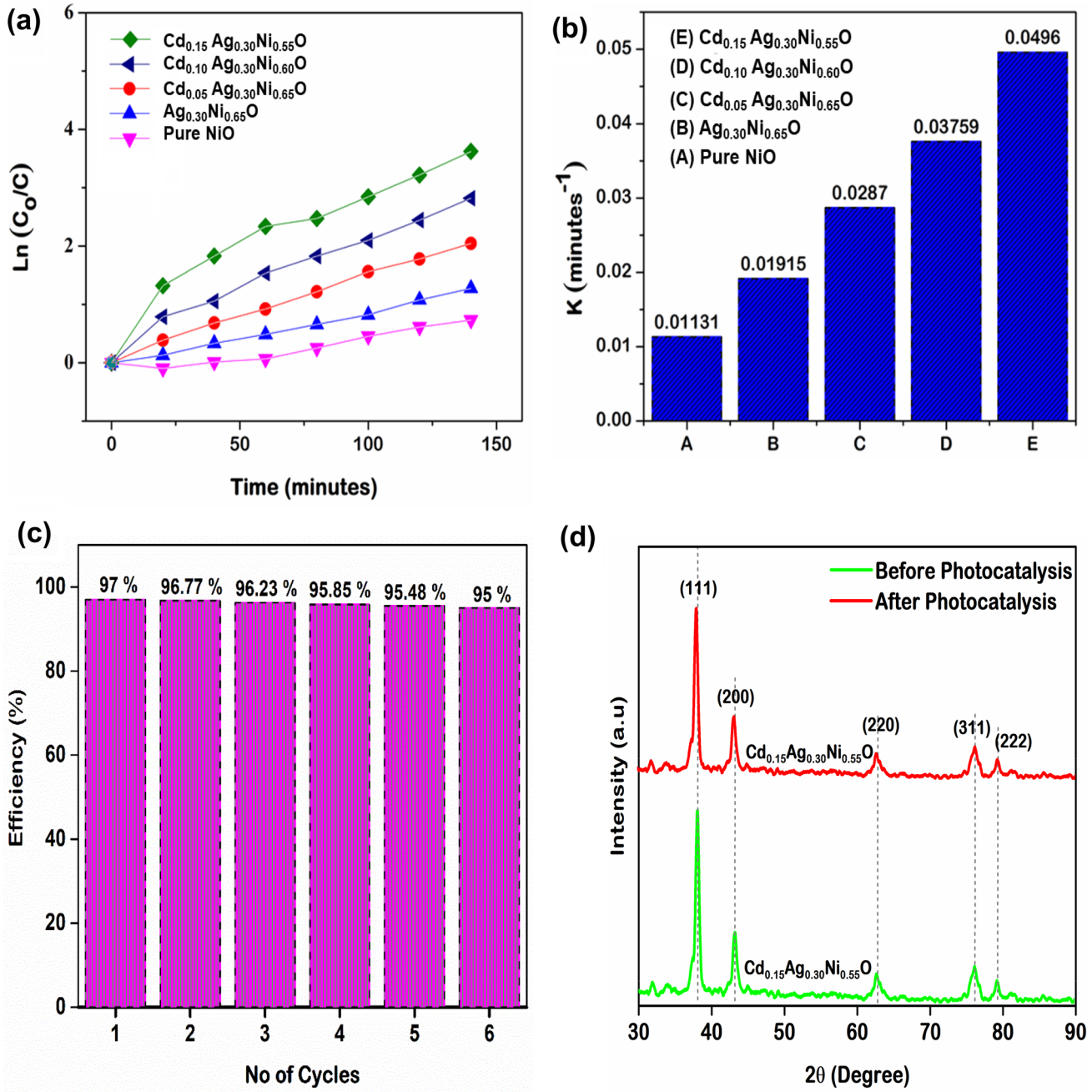

Fig. 10 Kinetic study of samples **a** plot of time versus ln(C0/C) for optimization of samples **b** reaction rate constant K (min^{-1}) for samples **c** reusability pattern of $Cd_{0.15}Ag_{0.30}Ni_{0.55}O$ for 6 cycles **d** XRD pattern of $Cd_{0.15}Ag_{0.30}Ni_{0.55}O$ for RhB dye before and after photocatalytic activity

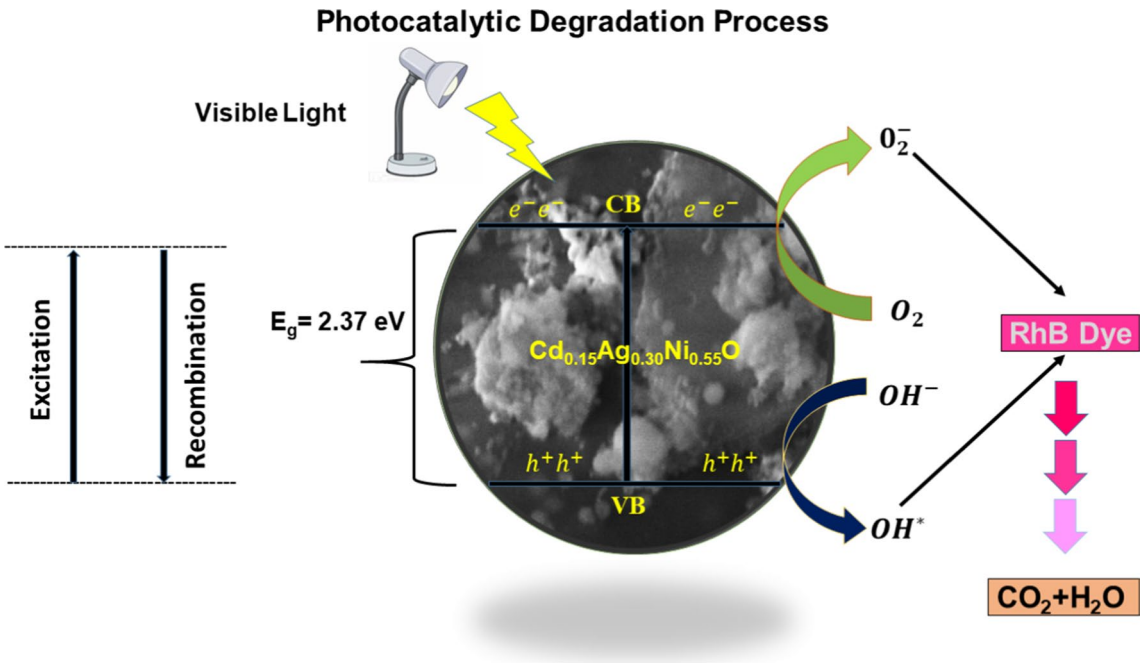

Fig. 11 Schematic mechanism for photocatalytic degradation of $Cd_{0.15}Ag_{0.30}Ni_{0.55}O$ for RhB dye

Table 3 Summary of characterization of data

Samples	Average crystallite size "d" (nm)	lattice parameter "a" (Å)	Efficiency (%)	Reaction rate constant *k* (min^{-1})
NiO	28	4.1772	24	0.01131
$Ag_{0.30}Ni_{0.70}O$	29	4.1753	39	0.01915
$Cd_{0.05}Ag_{0.30}Ni_{0.65}O$	26	4.1742	58	0.02870
$Cd_{0.10}Ag_{0.30}Ni_{0.60}O$	25	4.1701	79	0.03759
$Cd_{0.15}Ag_{0.30}Ni_{0.55}O$	24	4.1679	97	0.04960

This degradation study can be described further with the photocatalytic mechanism. In a typical mechanism, electron/hole pairs were generated at conduction and valance band of $Cd_{0.15}Ag_{0.30}Ni_{0.55}O$ when the sample was irradiated under visible light which had greater energy than the bandgap energy of this sample. The photocatalytic mechanism is shown in Fig. 11. These generated electrons (e^-_{cb}) react with electron acceptor oxygen O_2 and form a superoxide radical anion ($^{\bullet}O_2^-$). Similarly, valance band holes (h^+_{vb}) react with water H_2O adhering to sample surface, and hydroxyl radicals ($^{\bullet}OH$) are formed which are highly reactive (Pung et al. 2012; Tahir et al. 2020a). These hydroxyl radicals ($^{\bullet}OH$) and superoxide anions ($^*O_2^-$) react further with RhB dye and form degradation products H_2O and CO_2. The proposed reaction mechanism is given as follows:

$$Cd_xAg_{0.30}Ni_{0.70-x}O + h\upsilon\,(\text{visible}) \rightarrow e^-_{cb} + h^+_{vb} \quad (4)$$

$$e^-_{cb} + O_2 \rightarrow^{\bullet} O_2^- \quad (5)$$

$$h^+_{vb} + H_2O \rightarrow^{\bullet} OH + H^+ \quad (6)$$

$$^{\bullet}O_2^- + H_2O \rightarrow H_2O_2 + e^-_{cb} \rightarrow^{\bullet} OH \quad (7)$$

$$\text{RhB dye} + {}^{\bullet}\text{OH} + {}^{\bullet}\text{O}_2^- \rightarrow \text{H}_2\text{O} + \text{CO}_2. \quad (8)$$

At last, summary of all characterization data and photocatalytic performance is given in Table 3.

Conclusion

A series of samples comprising NiO and Ag–Cd co-doped NiO $Cd_xAg_{0.30}Ni_{0.70-x}O$ (X=0.0, 0.05, 0.10, and 0.15) have been synthesized successfully for the first time through the facile sol–gel technique, and their comparative photocatalytic performance for the decolorization of RhB dye under visible-light irradiation has been witnessed. XRD analysis confirmed the formation of NiO and co-doped NiO particles along with decrement in lattice constant "a" from 4.1772 Å to 4.1679 Å and crystallite size "d" from 28 to 24 nm with an increase in doping of Ag and Cd, respectively.

Among all of the as-synthesized samples, $Cd_{0.15}Ag_{0.30}Ni_{0.55}O$ showed the maximum degradation efficiency (97%) followed by first-order kinetics having reaction rate constant K (min^{-1}) 0.0496 with correlation coefficient (R^2) 0.988 as well as the excellent sustainability along with the reusability. Also, the sample $Cd_{0.15}Ag_{0.30}Ni_{0.55}O$ showed the shortest bandgap 2.37 eV as compared to NiO (3.20 eV). The best performance of this sample after a thorough comparison has been attributed to the shortest bandgap, delayed charge carrier recombination as well as the formation of energy levels between the conduction band and the valence band.

Acknowledgements The authors are very grateful to the Dr Khalid Nadeem Riaz and Dr. A. Dahshan for fruitful discussion on results and findings.

Declarations

Ethical approval This article does not contain any studies with human participants or animals performed by any of the authors

References

Ahmed R, Nabi G (2020) Morphology tailoring and enhanced electrochemical properties of Cd–Zn co-doped NiO nanorods for high performance supercapacitor. Ceram Int 46:22330–22337

Ahmed MB, Zhou JL, Ngo HH, Guo W, Thomaidis NS, Xu J (2017) Progress in the biological and chemical treatment technologies for emerging contaminant removal from wastewater: a critical review. J Hazard Mater 323:274–298

Al Boukhari J, Khalaf A, Sayed Hassan R, Awad R (2020) Structural, optical and magnetic properties of pure and rare earth-doped NiO nanoparticles. Appl Phys A 126:1–13

Al-Sehemi AG, Al-Shihri AS, Kalam A, Du G, Ahmad T (2014) Microwave synthesis, optical properties and surface area studies of NiO nanoparticles. J Mol Struct 1058:56–61

Amor MB, Boukhachem A, Labidi A, Boubaker K, Amlouk M (2017) Physical investigations on Cd doped NiO thin films along with ethanol sensing at relatively low temperature. J Alloy Compd 693:490–499

Anandan K, Rajendran V (2015) Effects of Mn on the magnetic and optical properties and photocatalytic activities of NiO nanoparticles synthesized via the simple precipitation process. Mater Sci Eng, B 199:48–56

Anwer H, Mahmood A, Lee J, Kim K-H, Park J-W, Yip ACK (2019) Photocatalysts for degradation of dyes in industrial effluents: opportunities and challenges. Nano Res 12:955–972

Arif M, Sanger A, Shkir M, Singh A, Katiyar RS (2019) Influence of interparticle interaction on the structural, optical and magnetic properties of NiO nanoparticles. Physica B 552:88–95

Aslam A, Razzaq A, Naz S, Amin N, Arshad MI, Nabi MAU, Nawaz A, Mahmood K, Bibi A, Iqbal F, Shakil M, Farooq Z, Iqbal MZ, Haider SS, Rehman AU (2021) Impact of lanthanum-doping on the physical and electrical properties of cobalt ferrites. J Superconduct Novel Magn 34:1–10

Ba-Abbad MM, Chai PV, Takriff MS, Benamor A, Mohammad AW (2015) Optimization of nickel oxide nanoparticle synthesis through the sol–gel method using box-Behnken design. Mater Des 86:948–956

Bashir B, Khalid MU, Aadil M, Zulfiqar S, Warsi MF, Agboola PO, Shakir I (2021) CuxNi1-xO nanostructures and their nanocomposites with reduced graphene oxide: synthesis, characterization, and photocatalytic applications. Ceram Int 47:3603–3613

Bibi R, Shen Q, Wei L, Hao D, Li N, Zhou J (2018) Hybrid BiOBr/UiO-66-NH2 composite with enhanced visible-light driven photocatalytic activity toward RhB dye degradation. RSC Adv 8:2048–2058

Chen Y, Zhu P, Duan M, Li J, Ren Z, Wang P (2019) Fabrication of a magnetically separable and dual Z-scheme PANI/Ag3PO4/NiFe2O4 composite with enhanced visible-light photocatalytic activity for organic pollutant elimination. Appl Surf Sci 486:198–211

Choudri BS, Al-Awadhi T, Charabi Y, Al-Nasiri N (2020) Wastewater treatment, reuse, and disposal-associated effects on environment and health. Water Environ Res 92:1595–1602

Crini G, Lichtfouse E (2019) Advantages and disadvantages of techniques used for wastewater treatment. Environ Chem Lett 17:145–155

Dehno Khalaji A (2015) Nickel Oxide (NiO) nanoparticles prepared by solid-state thermal decomposition of Nickel (II) Schiff base precursor. J Ultrafine Grained Nanostruct Mater 48:1–4

Deng X, Davé RN (2017) Breakage of fractal agglomerates. Chem Eng Sci 161:117–126

Deshpande MP, Patel KN, Gujarati VP, Patel K, Chaki SH (2016) Structural, thermal and optical properties of nickel oxide (NiO) nanoparticles synthesized by chemical precipitation method. Adv Mater Res 1141:65–71

Diallo A, Kaviyarasu K, Ndiaye S, Mothudi BM, Ishaq A, Rajendran V, Maaza M (2018) Structural, optical and photocatalytic applications of biosynthesized NiO nanocrystals. Green Chem Lett Rev 11:166–175

Din MI, Tariq M, Hussain Z, Khalid R (2020) Single step green synthesis of nickel and nickel oxide nanoparticles from Hordeum vulgare for photocatalytic degradation of methylene blue dye. Inorg Nano-Metal Chem 50:292–297

Ethiraj AS, Uttam P, Varunkumar K, Chong KF, Ali GAM (2020) Photocatalytic performance of a novel semiconductor nanocatalyst: copper doped nickel oxide for phenol degradation. Mater Chem Phys 242:122520

Fazlali F, Reza Mahjoub A, Abazari R (2015) A new route for synthesis of spherical NiO nanoparticles via emulsion nano-reactors with enhanced photocatalytic activity. Solid State Sci 48:263–269

OWA FD (2013) Water pollution: sources, effects, control and management. Mediterr J Soc Sci 4:65

Gawali SR, Dubal DP, Deonikar VG, Patil SS, Patil SD, Gomez-Romero P, Patil DR, Pant J (2016) Asymmetric supercapacitor based on nanostructured Ce-doped NiO (Ce: NiO) as positive and reduced graphene oxide (rGO) as negative electrode. ChemistrySelect 1:3471–3478

Ge J, Zhang Y, Heo Y-J, Park S-J (2019) Advanced design and synthesis of composite photocatalysts for the remediation of wastewater: a review. Catalysts 9:122

Gebreslassie G, Bharali P, Chandra U, Sergawie A, Boruah PK, Das MR, Alemayehu E (2019) Novel g-C3N4/graphene/NiFe2O4 nanocomposites as magnetically separable visible light driven photocatalysts. J Photochem Photobiol A Chem 382:111960

Ghazal S, Akbari A, Hosseini HA, Sabouri Z, Forouzanfar F, Khatami M, Darroudi M (2020) Biosynthesis of silver-doped nickel oxide nanoparticles and evaluation of their photocatalytic and cytotoxicity properties. Appl Phys A 126:1–8

Ghernaout D (2020) Advanced oxidation processes for wastewater treatment: facts and future trends. Open Access Libr J 7:1

Gogate PR, Pandit AB (2004) A review of imperative technologies for wastewater treatment II: hybrid methods. Adv Environ Res 8:553–597

Hameeda B, Mushtaq A, Saeed M, Munir A, Jabeen U, Waseem A (2021) Development of Cu-doped NiO nanoscale material as efficient photocatalyst for visible light dye degradation. Toxin Rev 40(4):1396–1406

Hussain M, Ceccarelli R, Marchisio DL, Fino D, Russo N, Geobaldo F (2010) Synthesis, characterization, and photocatalytic application of novel TiO_2 nanoparticles. Chem Eng J 157:45–51

Hussain K, Amin N, Arshad MI (2021) Evaluation of structural, optical, dielectric, electrical, and magnetic properties of Ce^{3+} doped $Cu_{0.5}Cd_{0.25}Co_{0.25}Fe_{2-x}O_4$ spinel nano-ferrites. Ceram Int 47:3401–3410

Jiang J, Oberdörster G, Biswas P (2009) Characterization of size, surface charge, and agglomeration state of nanoparticle dispersions for toxicological studies. J Nanopart Res 11:77–89

Kannan K, Radhika D, Nikolova MP, Sadasivuni KK, Mahdizadeh H, Verma U (2020) Structural studies of bio-mediated NiO nanoparticles for photocatalytic and antibacterial activities. Inorg Chem Commun 113:107755

Kerli S, Soğuksu AK, KAVGACı, M. (2020) Production of nickel oxide nanostructure particles and their photocatalytic degradation of different organic dye. Int J Mod Phys B 34:2050081

Khairnar SD, Shrivastava VS (2019) Facile synthesis of nickel oxide nanoparticles for the degradation of Methylene blue and Rhodamine B dye: a comparative study. J Taibah Univ Sci 13:1108–1118

Khan AH, Khan NA, Ahmed S, Dhingra A, Singh CP, Khan SU, Mohammadi AA, Changani F, Yousefi M, Alam S (2020) Application of advanced oxidation processes followed by different treatment technologies for hospital wastewater treatment. J Clean Prod 269:122411

Khatri A, Rana PS (2019) Visible light photocatalysis of methylene blue using cobalt substituted cubic NiO nanoparticles. Bull Mater Sci 42:1–11

Khatri A, Rana PS (2020) Visible light assisted photocatalysis of Methylene Blue and Rose Bengal dyes by iron doped NiO nanoparticles prepared via chemical co-precipitation. Physica B 579:411905

Khodair ZT, Al-Jubbori MA, Shano AM, Sharrad FI (2020) Study of optical and structural properties of (NiO) 1–x (CuO) x nanostructures thin films. Chem Data Collect 28:100414

Ma J, Ding Z, Wei G, Zhao H, Huang T (2009) Sources of water pollution and evolution of water quality in the Wuwei basin of Shiyang river, Northwest China. J Environ Manage 90:1168–1177

Malik R, Tomer VK, Joshi N, Dankwort T, Lin L, Kienle L (2018) Au–TiO_2-loaded cubic g-C3N4 nanohybrids for photocatalytic and volatile organic amine sensing applications. ACS Appl Mater Interfaces 10:34087–34097

Mansour S, Knani S, Bensouilah R, Ksibi Z (2020) Wastewater problems and treatments. Current Trends and Future Developments on (Bio-) Membranes Chapter 8:151–174

Medhi R, Marquez MD, Lee TR (2020) Visible-light-active doped metal oxide nanoparticles: review of their synthesis, properties, and applications. ACS Appl Nano Mater 3:6156–6185

Mohammadyani D, Hosseini SA, Sadrnezhaad SK (2012) Characterization of nickel oxide nanoparticles synthesized via rapid microwave-assisted route. Int J Modern Phys Conf Ser 05:270–276

Murali A, Sarswat PK, Free ML (2020) Minimizing electron-hole pair recombination through band-gap engineering in novel ZnO-CeO_2-rGO ternary nanocomposite for photoelectrochemical and photocatalytic applications. Environ Sci Pollut Res Int 27:25042–25056

Palanivel B, Shkir M, Alshahrani T, Mani A (2021) Novel NiFe2O4 deposited S-doped g-C3N4 nanorod: Visible-light-driven heterojunction for photo-Fenton like tetracycline degradation. Diamond Related Mater 112:108148

Palma P, Alvarenga P, Palma VL, Fernandes RM, Soares AMVM, Barbosa IR (2010) Assessment of anthropogenic sources of water pollution using multivariate statistical techniques: a case study of the Alqueva's reservoir, Portugal. Environ Monit Assess 165:539–552

Pellegrino F, Pellutiè L, Sordello F, Minero C, Ortel E, Hodoroaba V-D, Maurino V (2017) Influence of agglomeration and aggregation on the photocatalytic activity of TiO_2 nanoparticles. Appl Catal B 216:80–87

Puckett LJ (1995) Identifying the major sources of nutrient water pollution. Environ Sci Technol 29:408A-414A

Pung S-Y, Lee W-P, Aziz A (2012) Kinetic study of organic dye degradation using ZnO particles with different morphologies as a photocatalyst. Int J Inorg Chem 2012:608183

Rahman MA, Radhakrishnan R, Gopalakrishnan R (2018) Structural, optical, magnetic and antibacterial properties of Nd doped NiO nanoparticles prepared by co-precipitation method. J Alloy Compd 742:421–429

Rahman A, Aadil M, Akhtar M, Warsi MF, Jamil A, Shakir I, Shahid M (2020) Magnetically recyclable $Ni_{1-x}Cd_xCe_yFe_{2-y}O_4$-rGO nanocomposite photocatalyst for visible light driven photocatalysis. Ceram Int 46:13517–13526

Ranjbar M, Taher MA, Sam A (2015) NiO nanostructures: novel solvent-less solid-state synthesis, characterization and MB photocatalytic degradation. J Mater Sci Mater Electron 26:8029–8034

Rosenwinkel K.-H., Austermann-Haun U, Meyer H (2005) Industrial wastewater sources and treatment strategies. Environmental Biotechnology: Concepts and Applications Chapter 2:49–77

Sacco O, Vaiano V, Rizzo L, Sannino D (2018) Photocatalytic activity of a visible light active structured photocatalyst developed for municipal wastewater treatment. J Clean Prod 175:38–49

Sagadevan S, Podder J (2015) Investigations on structural, optical, morphological and electrical properties of nickel oxide nanoparticles. Int J Nanopart 8:289–301

Shakil M, Inayat U, Arshad MI, Nabi G, Khalid NR, Tariq NH, Shah A, Iqbal MZ (2020) Influence of zinc and cadmium co-doping on optical and magnetic properties of cobalt ferrites. Ceram Int 46:7767–7773

Shannon MA., Bohn PW, Elimelech M., Georgiadis JG, Marinas BJ, Mayes AM (2010) Science and technology for water purification in the coming decades. Nanoscience and technology: a collection of reviews from nature journals. World Scientific, Singapore. 452:337–346

Sheena PA, Priyanka KP, Sabu B, Varghese T (2014) Effect of calcination temperature on the structural and optical properties of nickel oxide nanoparticles. Nanosyst Phys Chem Math 5:441–449

Shekofteh-Gohari M, Habibi-Yangjeh A (2017) Fe3O4/ZnO/CoWO4 nanocomposites: novel magnetically separable visible-light-driven photocatalysts with enhanced activity in degradation of different dye pollutants. Ceram Int 43:3063–3071

Tahir MB, Nabi G, Khalid NR, Khan WS (2018) Synthesis of nanostructured based WO_3 materials for photocatalytic applications. J Inorg Organomet Polym Mater 28:777–782

Tahir MB, Ashraf M, Rafique M, Ijaz M, Firman S, Mubeen I (2020a) Activated carbon doped WO_3 for photocatalytic degradation of rhodamine-B. Appl Nanosci 10:869–877

Tahir MB, Riaz KN, Rafique M, Rafique MS, Yousaf N, Sagir, M (2020b) Photocatalysis fundamentals. Nanotechnology and photocatalysis for environmental applications. Elsevier chapter 4:57–64

Torki F, Faghihian H (2018) Visible light degradation of naproxen by enhanced photocatalytic activity of NiO and NiS, scavenger study and focus on catalyst support and magnetization. Photochem Photobiol 94:491–502

van Loosdrecht MCM, Nielsen PH, Lopez-Vazquez CM, Brdjanovic D (2016) Experimental methods in wastewater treatment. IWA publishing, London

Yongabi KA (2010) Biocoagulants for water and waste water purification: a review. Int Rev Chem Eng 2:444–458

Zahra T, Ahmad KS, Ali D (2020) Ecospheric decontamination attained via green nanobiotechnological NiO-based nanocatalyst derived from nature's biofactories. Int J Nanomed 15:8357